Journal of Geodesy manuscript No.
(will be inserted by the editor)

Astronomy VLBA campaign MOJAVE used in geodesy

Hana Krásná · Leonid Petrov

Received: date / Accepted: date

Abstract **Keywords** First keyword · Second keyword · More

1 Introduction

Group delay of an extended source observed with very long baseline interferometry (VLBI) differs from the group delay of the point source. Up to now, the contribution of source structure is not included in routine analysis of VLBI data. It was known for long time that source structure is a significant (f.e., **Zeppenfeld, 1993**; **Sovers et al., 2002**; **Tornatore and Charlot, 2007**; **Shabala et al., 2015**; **Petrov and Kovalev, 2017**) or even the major contributor (**Anderson and Xu, 2018**) to the error budget in geodetic VLBI. Corr 1

One of the most promising ways to compute the source structure contribution to group delay is to generate images from the same VLBI observations, perform their 2D Fourier transform over spatial coordinates, and use it for calculations (see, f.e., **Petrov and Kovalev, 2017**). Unfortunately, geodetic observing schedules are not well suited for producing good quality images. A typical geodetic schedule splits the network into a number of ad hoc subarrays, so a subset of stations observes one source and a subset of other stations observes another source at the same time and upon completion of integration, another subset of stations observe the next source. This leads to a very substantial reduction of the number of closures in phase and amplitudes required for robust imaging. Astronomical schedules usually avoid subarrays. The use of data for geodesy and astrometry from astronomical programs designed for imaging was not common in the past because 4 to 8 intermediate recorded frequencies were usually allocated contiguously, while for geodetic applications the frequencies are allocated as wide as possible. As a result, group delay uncertainty at a given signal to noise ratio (SNR) was an order of magnitude worse than from geodetic schedules and although these such data were still useful for astrometry (**Petrov, 2011, 2013**), they were not interesting for geodesy. A non-contiguous allocation of intermediate frequencies for astronomy projects was rare because usually it was not required and a commonly used AIPS software package (**Greisen, 2003**) that implemented the fringe fitting procedure dos not support processing these data. data. In a case if the goal of astronomical observation required wide spanned band width, for instance, for VLBA Imaging and Polarimetry Survey at 5 GHz (**Helmboldt et al., 2007**), processing the data in a geodetic mode was feasible provided good results (**Petrov and Taylor, 2011**). However, single-band observations at rather low frequencies such as 5 GHz are affected by the ionospheric contribution and this limits their usability for geodesy. Corr 2

H. Krásná
1. TU Wien, Department of Geodesy and Geoinformation, Wien, Austria
2. Astronomical Institute of the Czech Academy of Sciences, Prague, Czech Republic
E-mail: hana.krasna@tuwien.ac.at

L. Petrov
NASA Goddard Space Flight Center, Code 61A, Greenbelt, USA

Progress in radioastronomy instrumentation resulted in an increase of recorded bandwidth. Since 2016–2020, astronomical observations typically cover frequency band 256 or 512 MHz which produce group delay precision on par with geodetic setups. Therefore, an astronomical observing program suitable as a testbed for studying source structure contribution in detail should a) observe strong sources; b) be conducted at rather high frequencies to minimize the impact of the ionosphere. MOJAVE-5 (Monitoring Of Jets in Active galactic nuclei with VLBA (Very Long Baseline Array) Experiments) suits both these criteria. The program commenced in 1994 Lister et al. (2018) and focused on observations of bright active galactic nuclea (AGNs) with discernible structure at 15 GHz. Corr 3

MOJAVE (Monitoring Of Jets in Active galactic nuclei with VLBA (Very Long Baseline Array) Experiments) is a long-term program carried out by an astrophysics community, which focuses on monitoring of radio brightness and polarization variations in jets associated with active galaxies on parsec-scales visible in the northern sky (Lister et al., 2018). In September 2016 the observing series with the VLBA observation code "bl229" has started. In this series, the observations are carried out at a wavelength of 2 cm (15 GHz, Ku band) approximately every month within 2048 Mbps 24 hour-long experiments.

The MOJAVE dataset provides a unique testbed for research of source structure which is recognized as one of the contributors (Sovers et al., 2002; Tornatore and Charlot, 2007; Shabala et al., 2015) or even as the major contributor (Anderson and Xu, 2018) to errors in geodetic VLBI.

The Earth orientation parameters, which built the link between the terrestrial and celestial reference frame, are regularly estimated by Very Long Baseline Interferometry. The unsubstitutable role of VLBI is in the measurement of UT1-UTC and nutation components. Until recently, the estimates of EOP were produced only from the observations in the traditional S/X bands (2.3/8.6 GHz, 13/3.6 cm). In Krásná et al. (2019) the first estimates of the EOP from the dedicated geodetic VLBA experiments in K band (24 GHz, 1.2 cm) were published. In this paper, we present the first EOP estimates in Ku band (15 GHz, 2 cm) from purely astrophysics VLBA sessions covering the last four years (2016.7 — 2020.5). In Krásná and Petrov (2021, in preparation) we further focus on the MOJAVE data from the astrometry point of view, dealing with the estimated radio source positions which built the celestial reference frame.

2 Motivation

Before commencing a thorough investigation of the impact of source structure on astrometry and geodesy results we need establish a solid foundation of that work. MOJAVE dataset differs by a) the way how it was scheduled; b) by observing frequencies; and c) by the source selection. Corr 4

An observing schedule consists of a sequence of time intervals called scans when all or a part of antennas of the network record voltage from a given source. Astronomical schedules are usually made by optimization of the uv-coverage, i.e. projections of the baseline vector on the plane tangential to the source direction. The goal is to generate such a sequence of observations that covers that plane as uniform as possible for each program source. Geodetic schedules are usually made to optimize elevation/azimuth coverage at each station for some interval (1–3 hours). Corr 5

Geodetic observations are done at two or more frequencies simultaneously. Since the ionospheric group delay is frequency dependent, multi-band observations allows to derive an ionosphere free combination of group delays. Astronomical observations are usually done at one frequency at once. Therefore, group delay observables form astronomical observations are affected by the ionosphere. Corr 6

A list of $\sim$100 objects are usually observed with geodesy schedules. Sources with extended structures are observed less often than point-like sources. Astronomical schedules have less sources, but they are observed more intensively during an experiment. Sources with extended structures are preferably picked. Corr 7

In this paper we wanted to answer the following questions: 1) what are the metrics of geodetic parameters from MOJAVE-5 dataset? 2) how worse or better these metrics are with respect to similar geodetic programs? 3) what is the main cause of these differences? And finally, we wanted to learn whether we can use MOJAVE-5 dataset as a testbed for investigation of the impact of source structure on geodetic and astrometric results. Corr 8

3 Data analysis

The VLBA network consists of ten 25-meters radio telescopes located on the U.S. territory (eight in North America, one in the Pacific, and one in the Caribbean), see Fig. 1. The **interferometric visibility data of** MOJAVE-5 campaign (observing code bl229) at **15.3 GHz (Ku band), dual circular polarization,** ~~from the VLBA correlator~~ are publicly available through the National Radio Astronomy Observatory (NRAO) Science Data archive[1] in the FITS-IDI (Interferometry Data Interchange) format. ~~This observing series started on September 26, 2016 and we include the first 33 experiments with the last one on July 02, 2020 in this publication.~~ **We processed 33 MOJAVE-5 experiments since September 26, 2016 through July 02, 2020**.

~~In~~ The first 25 experiments (bl229aa-ay) were observed at eight ~~sub-bands~~ **independent recorded eight intermediate frequencies (IF) of 32 MHz wide per polarization using the PFB personality of the digital backend.** ~~64 channels each~~. Since July 2019 (experiment bl229az) ~~the bandwidth of a sub-band has increased to 64 MHz, which built four sub-bands covering 128 channels~~ **MOJAVE-5 campaign used four IFs of 64 MHz wide per polarization using the DDC personality of the digital backend. In both cases the total recorded bandwidth per polarization was 256 MHz** (see Table 1). We processed the observations with the fringe-fitting software PIMA (Petrov et al., 2011) (coarse fringe fitting – bandpass calibration – fine fringe fitting) and produced databases including among others group delays and their uncertainties. ~~in a geo-VLBI format GVH and its plain ascii database counter-part VGOSDA, or for short VDA~~ footnotehttp://astrogeo.org/gvh/vda. These **quantities** ~~databases~~ serve as input for the data analysis software package pSolve[2] and as an alternative input for the analysis software package VieVS (Böhm et al., 2018).

We process the MOJAVE group delays with these two independent analysis software packages and compare the estimated baseline lengths and Earth orientation parameters in terms of the weighted root mean square. ~~Furthermore,~~ **As a reference dataset**, we analyzed 22 geodetic RV ~~(Research and Development VLBI)~~ **(Regular geodesy with VLBI) (Petrov et al., 2009)**- and 6 CN sessions observed in S/X band for the same time span starting with rv119 on September 14, 2016 ~~until RDV141 on~~ through July 07, 2020. ~~which are 22 RDV and 6 CN experiments in total. RV sessions are astrometric/geodetic sessions scheduled for full ten stations VLBA network plus up to ten geodetic stations capable of recording VLBA modes.~~ **The RV network consists of ten VLBI and three to six other geodetic stations.** These sessions are scheduled to provide ~~among others~~ accurate EOP, a high accuracy TRF, **and source positions**. ~~where the VLBA stations are incorporated into the VLBI reference frame through the inclusion of other geodetic stations with long history of observations.~~ **Only 10 VLBA stations participated in CN experiments.** ~~The CN experiments consist of the ten VLBA stations only and run concurrent with the Rapid turnaround Monday IVS sessions (IVS-R1).~~ We show the comparison of the baseline length scatter between the VLBA telescopes and of the estimated EOP from the astrophysics MOJAVE measurements and from the dedicated geodetic experiments.

~~Besides the comparison of the estimated geodetic parameters from two diverse VLBA datasets, we take the opportunity to examine the differences in the estimated parameters due to the use of different software packages.~~ ~~Therefore,~~ **As an extra check,** we analyzed the VLBA data in several ways. One solution was produced using the software PIMA for the fringe-fitting and pSolve for the analysis. In the second solution we analyzed the group delays produced with the PIMA software with the analysis software VieVS. For the rv+cn experiments we run another solution them with the software VieVS where we used ~~the official vgosDB databases maintained by the International VLBI Service for Geodesy~~

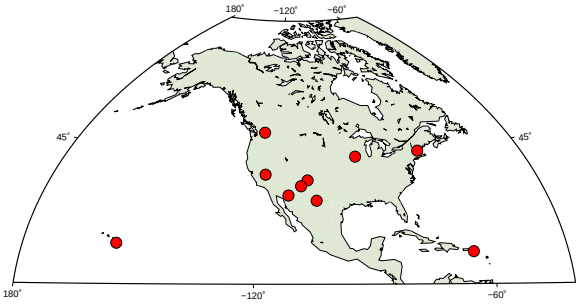

Fig. 1 Distribution of the ten VLBA radio telescopes.

Table 1 Lower edge frequency of the sub-bands in the bl229 experiments in GHz.

bl229aa–ay	bl229az–bg
15.22400	15.17575
15.25600	15.25575
15.28800	15.31975
15.32000	15.38375
15.35200	
15.38400	
15.41600	
15.44800	

[1] https://archive.nrao.edu/archive
[2] http://astrogeo.org/psolve

~~& Astrometry (IVS)~~ **group delays evaluated with Fourfit visibility analysis software. These data products were retrieved from the International VLBI Service for Geodesy & Astrometry (IVS) data archive[3].** Corr 21

Tables 2 and 3 contain the parameterization of the estimated parameters in the solutions. The MOJAVE and RDV&CN experiments are processed in the same manner with the same parameterization to allow for an informative comparison.

Baseline length repeatability. We run several solutions which we compare in terms of baseline scatter. In Fig. 2 we show the Noteweighted root mean squares (wrms) of the estimated baseline length from selected solutions computed with pSolve (upper figure) and with VieVS (lower figure). In both figures the red crosses denote the baselines determined from the MOJAVE experiments. Two further solutions in the upper figure compare the baseline scatter computed from the RDV&CN sessions once with the whole scheduled network and once with observations conducted at the VLBA stations only. The results show that ~~neglecting~~ **dropping** the data obtained with the non-VLBA stations does not change the wrms of the baseline lengths between the VLBA telescopes. In the lower plot we compare the MOJAVE bl229 baseline scatter with rv+cn sessions ~~pre-processed and provided as the official vgosDB database by the IVS.~~ processed with Fourfit. Comparison of the VLBA baseline scatter obtained from MOJAVE and RDV&CN sessions gives similar conclusion independently from the used software packages. There is an increase in the baseline length repeatability from a solution using the MOJAVE-5 dataset with respect to the reference RDV&CN sessions. With a linear approximation the difference makes about 1.3 mm for a 1000 km long baseline or 3.2 mm for 8000 km baseline length. The coefficients of the linear regression are summarized in Table 4. **We conclude the baseline length repeatability derived from analysis of single-bane 15 GHz MOJAVE-5 experiments is approximately a factor of 1.5 greater than these statistics derived from contemporary dual-band 2/8 GHz datasets.** Corr 22 Corr 23

Earth orientation parameters The Earth orientation parameters are estimated in a so-called backward solution, i.e., a solution consistent with globally estimated terrestrial and celestial reference frame from the respective sessions. The orientation of the TRF is set with the NNT/NNR condition on all ten VLBA stations and the CRF is oriented with the NNR condition on ICRF3 defining sources. Several solutions similar to that introduced in the afore-noted paragraph are computed and the EOP are estimated with both software packages pSolve and VieVS. Table 5 shows the wrms of the ERP (polar motion components and dUT1) w.r.t. IERS 14 C04 time series after a trend and bias removal, whereas the wrms of the nutation offsets is given w.r.t. a harmonic expansion heo_20200606.heo **produced from analysis of available geodetic VLBI data since 1980 through 2020 using the method presented in Petrov (2007)**. In addition the median formal error for all five EOP is summarized in the table. We show three solutions computed with pSolve similar to those introduced by the baseline length repeatability, i.e., EOP from MOJAVE dataset, EOP from RDV&CN sessions including all stations, and EOP from RDV&CN sessions using the VLBA telescopes only. **Estimation of EOP using single band observations at high frequencies was made in the past (f.e., Petrov et al., 2011). Our recent processing of of 37 VLBA experiments at 24 GHz (Krásná et al., 2019) showed that although formal uncertainties were on par with dual-band regular geodetic experiments (60 μas for X-pole, 80 μas for Y pole and 5μs for UT1), wrms of difference with respect to the IERS 14 C04 time series taken as a reference were greater than formal uncertainties by a factor of 3 for polar motion and a factor of 10 for UT1.** Corr 24 Corr 25

Table 5 shows that EOP determined from MOJAVE-5 data have the wrms differences with respect to the reference IERS 14 C04 a factor of 1.3 to 1.8 larger than from RV+CN experiments at the same network. Corr 26

4 Differences between MOJAVE bl229 and RDV&CN

We recognize that there are three major differences between the datasets which can have an impact on the geodetic results. The first one is the scheduling approach due to different goals of the experiments. The second one is the treatment of ionosphere since MOJAVE-5 sessions are single-band experiments. The third difference lies in the radio sources which were selected for observations. **We will try to isolate these factors and determine which factor has the greatest impact on the accuracy of geodetic solutions.** Corr 27

[3] Available at https://ivscc.gsfc.nasa.gov/products-data/index.html

Table 2 Parameterization of estimated parameters of the single session solutions in pSolve

	pSolve
CRF	selected sources ~~with constraint sigma 20 as~~
TRF	NNT/NNR condition on VLBA stations with 0.1 mm constraints
ERP	offset and rate ~~with constraint sigma 45 mas (3 ms) on offset~~
celestial pole offsets	offset without constraints
zenith wet delay	B-spline with the time span 20 min and sigma of constraints 50.00 ps/h
tropo. gradients	8 hours with sigma of constr. 0.5 mm on offset and 2.00 mm/day on rate
clocks	B-spline with the time span 60 min and constraint sigma 5.e-14 s/s
baseline clock offsets	offset with constraint sigma 500 ns
weights	yes

Table 3 Parameterization of estimated parameters of the single session solutions in VieVS

	VieVS
CRF	selected sources without constraints
TRF	NNT/NNR condition on VLBA stations
ERP	pwlo with the time span 24 hours with relative constraints 1 mas
celestial pole offsets	offset
zenith wet delay	pwlo with time span 30 min with relative constraints 1.5 cm
tropo. gradients	pwlo with time span 180 min with relative constraints 0.5 cm
clocks	pwlo with time span 60 min with relative constraints 1.3 cm, one rate and one quadratic term
baseline clock offsets	offset without constraints
weights	baseline-dependent weighting

Table 4 Baseline length scatter. Coefficients of a linear regression: $a \cdot L + b$ where L is length of baseline in [mm].

dataset	software	a [ppb]	b [mm]
MOJAVE bl229	PIMA, pSolve	0.91	2.50
RDV&CN VLBA only	PIMA, pSolve	0.64	1.51
RDV&CN all stat	PIMA, pSolve	0.61	1.54
MOJAVE bl229	PIMA, VieVS	0.98	2.04
RDV&CN all stat	vgosDB, VieVS	0.60	1.17

4.1 Scheduling

In Fig. 3 we show the sky coverage during a 24-hour observing session at three selected telescopes (BR-VLBA, FD-VLBA, SC-VLBA) where colors depict the time passed since the start of the session. As an example we show the sky coverage during the MOJAVE session bl229bc observed on December 22, 2019 in the upper plots and the CN1924 session observed with the same network on December 09, 2019 in the lower plots. Table 7 summarizes the mean number of scans in a 24-hour experiment at each of the ten VLBA telescopes computed over the investigated time period (September 2016 — July 2020). The numbers show, that during geodetic experiments there are twice as many scans at each telescope as during the MOJAVE sessions. The geodetic sessions focus on even distribution of the observations over all azimuth and elevation angles in the common visibility sky area to ensure a good decorrelation of station dependent parameters such as station height, zenith wet delay, clock parameters or baseline clock offsets. On the other hand, the primary goal of the bl229 experiments is **to provide best images** ~~in monitoring~~ of jets in active galactic nuclei, therefore the schedule is optimized to track a set of sources in a 24-hour session. The Fig. 4 depicts the total number of observed sources in each session (upper plot) and the median number of observations during a 24-hour session for each source computed over the respective four years period. The red crosses show the MOJAVE sessions, and blue x-signs depict the RDV&CN sessions. The median of observed sources lies at 30 radio sources during a MOJAVE session, and at 78 radio sources during a RDV&CN session. Comparison of the number of observations for each source during a whole session shows that 95% of the AGN observed in MOJAVE sessions have more than 150 observations whereas only 35% of the sources observed in RDV&CN sessions gets over this limit. ~~This shows again the interest of MOJAVE sessions to obtain enough data for particular sources during an experiment to allow for imaging and astrophysics study~~. Sources with few observations in geodetic experiments serve for a good sky coverage over the stations which allows an accurate estimation of geodetic relevant parameters.

Corr 28

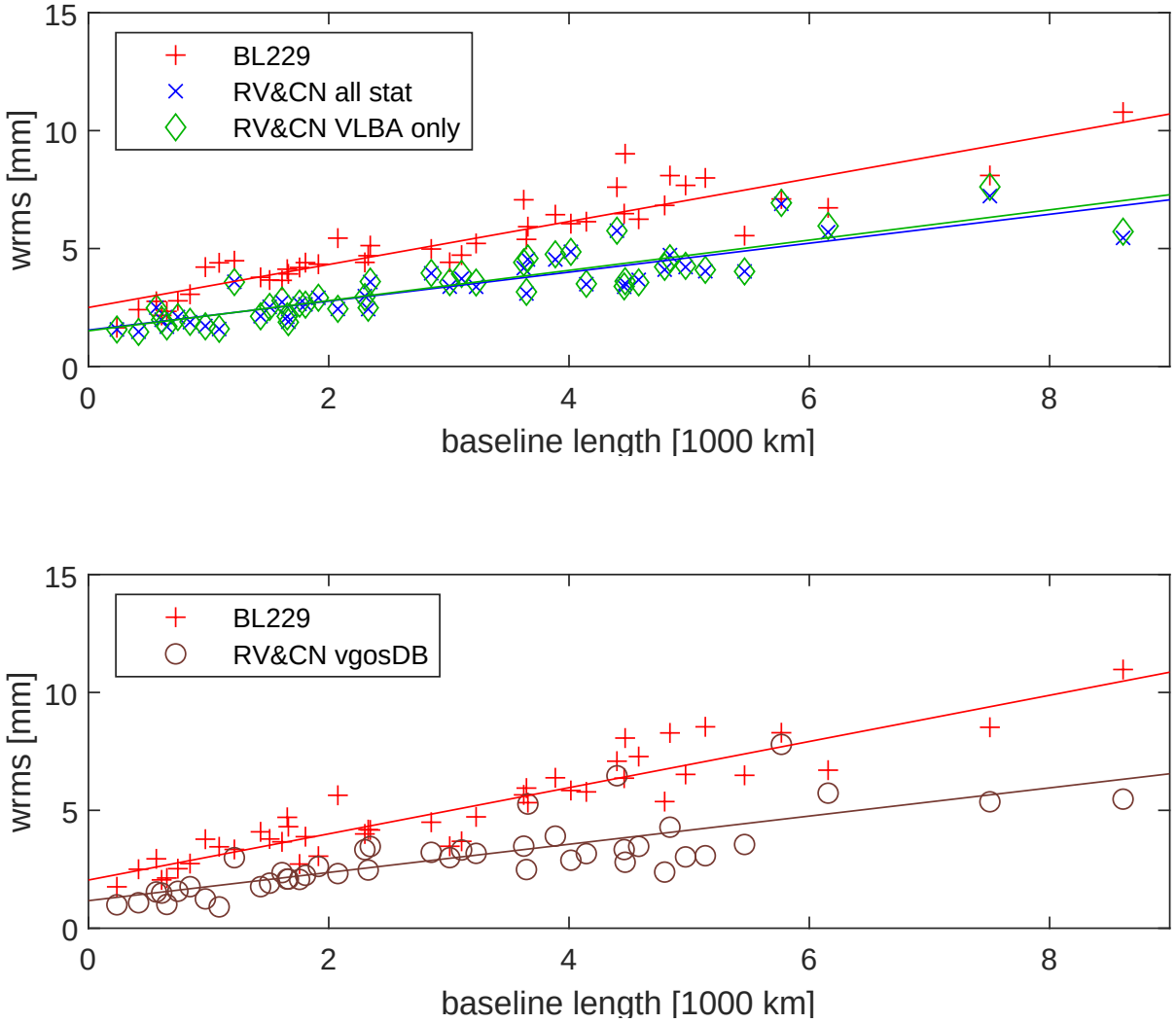

Fig. 2 Baseline length scatter. Without iono correction.

Table 5 Statistics (wrms and median formal error) of the estimated EOP from MOJAVE bl229 and RDV&CN series. The values for ERP are given w.r.t. IERS 14 C04 time series after trend and bias removal, for celestial pole offsets dX and dY w.r.t. harmonic expansion heo_20200606.heo

		x-pole [μas]	y-pole [μas]	dUT1 [μs]	dX [μas]	dY [μas]
MOJAVE bl229	wrms	228	286	23	169	128
	median formal error	109	153	9	59	56
RDV&CN VLBA only	wrms	126	218	15	89	129
	median formal error	80	120	6	92	69
RDV&CN all stat	wrms	117	130	14	72	87
	median formal error	57	89	4	86	60

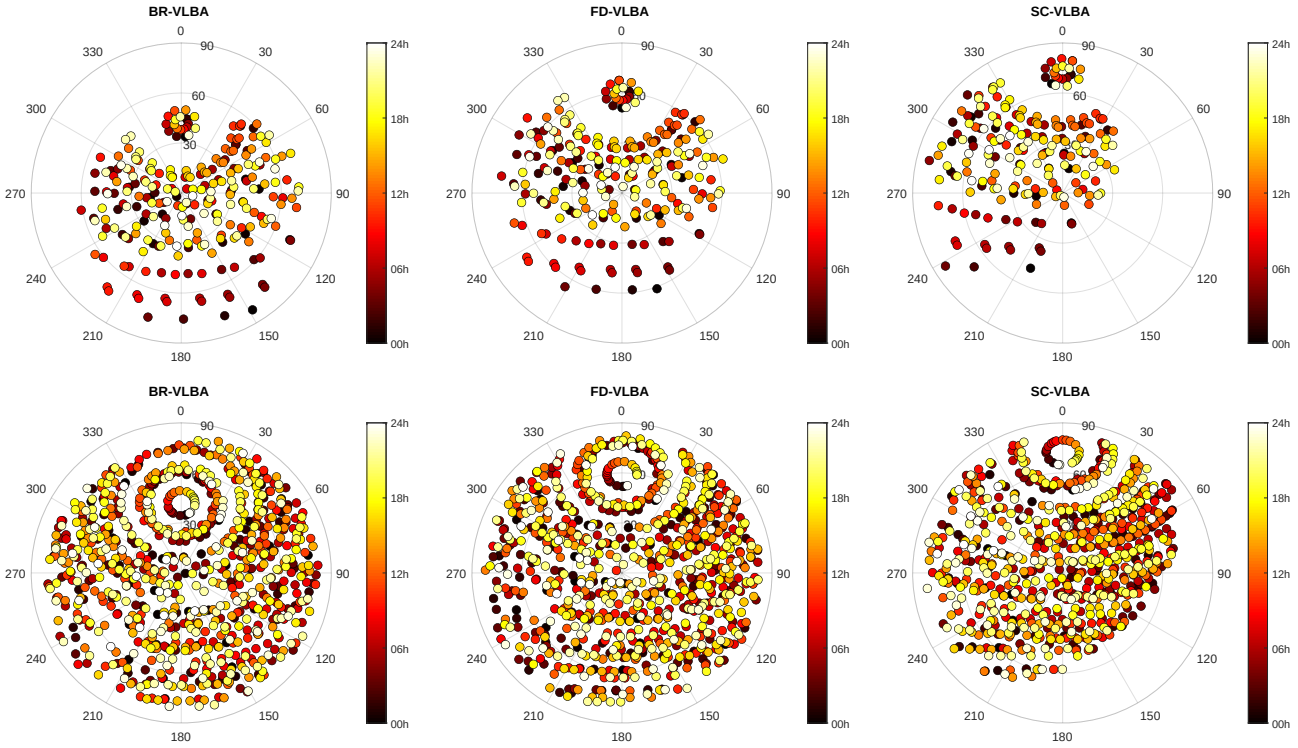

Fig. 3 Sky coverage of three VLBA stations: BR-VLBA, FD-VLBA and SC-VLBA during the bl229bc MOJAVE experiment (upper plots) and the CN1924 experiment (lower plots).

Table 6 Weighted rms of post fit residuals in [ps].

	min	max	median
MOJAVE bl229 series	11.3	28.7	18.4
geodetic RDV&CN all stat	14.7	40.3	25.2
geodetic RDV&CN vlba only	14.7	37.8	24.1

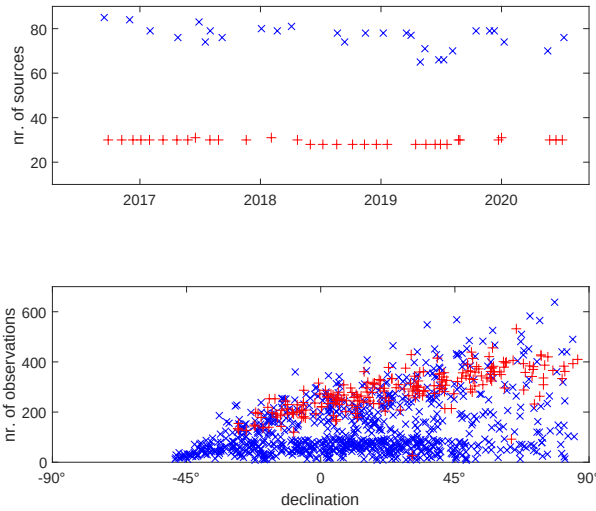

Fig. 4 The upper plot shows number of observed sources in each session. The lower plot depicts the median number of observations for each source. The red crosses stand for the bl229 experiments, blue x-signs for the RDV&CN experiments.

4.2 Ionosphere

The ionosphere is a refractive media. Propagating in the ionosphere, phase delay decreases, and group delay τ_{gr} increases with respect to the ionosphere free τ_{if} group delay in the absence of the ionosphere as

$$\tau_{gr} = \tau_{if} + \kappa \Delta\mathrm{TEC}/f_{\mathrm{eff}}^2, \qquad (1)$$

where f_{eff} is the effective frequency that is within several percent from the recorded central sky frequency, ΔTEC is the differential Total Electron Content measured in TEC units (TECU, 1 TECU $= 10^{16}$ electron/m^2):

$$\Delta\mathrm{TEC} = \int N_v \, ds_1 - \int N_v \, ds_2 \qquad (2)$$

with s_1 and s_2 as paths of wave propagation from a source to the first and second station of the radio interferometer, and

$$\kappa = 10^{-16} \cdot \frac{e^2}{2\,\mathrm{c}\, m_e\, \epsilon_o} = 5.308018 \cdot 10^{10}\ \mathrm{s}^{-1} \qquad (3)$$

Table 7 Mean number of scans at VLBA telescopes in one session computed over the period of interest (September 2016 - July 2020).

	Br	Fd	Hn	Kp	La	Mk	Nl	Ov	Pt	Sc
MOJAVE bl229 series	245	245	241	248	251	204	251	252	235	219
geodetic RDV&CN experiments	451	485	445	493	483	357	467	487	451	423

where e — charge of an electron, m_e — mass of an electron, ϵ_o — permittivity of free space, c — velocity of light in vacuum.

To mitigate the impact of the ionosphere on group delay, geodetic observations are usually conducted at two frequencies simultaneously. Combining group delays τ_u and τ_l at the upper and lower frequencies f_u and f_l respectively, we can derive the differential TEC and the ionosphere free path delay as

$$\begin{aligned} \Delta TEC &= \frac{f_u^2 f_l^2}{f_u^2 - f_l^2}\,(\tau_l - \tau_u), \\ \tau_{if} &= \frac{f_u^2}{f_u^2 - f_l^2}\,\tau_u - \frac{f_l^2}{f_u^2 - f_l^2}\,\tau_l, \\ \tau_{iu} &= \frac{f_l^2}{f_u^2 - f_l^2}\,(\tau_l - \tau_u). \end{aligned} \tag{4}$$

Derivations of these equations can be found for example in Petrov et al. (2011). This approach allows to effectively cancel the ionospheric contribution, leaving residual contribution at a level not exceeding several picoseconds (Hawarey et al., 2005).

MOJAVE program used only one frequency. An alternative approach for modeling the ionospheric contribution is to use TEC maps from GNSS observation processing. Applying time and spacial interpolation, we can compute TEC in the up direction for each station and each observation. Then we can related the TEC into direction of observation at elevation angle E to TEC in vertical direction via mapping function $M_i(E)$. Considering the ionosphere as a thin shell at height H, we can easily derive the mapping function as

$$\begin{aligned} M_i(E) &= \frac{1}{\cos\beta(E)}, \\ \beta(E) &= \arcsin\frac{\cos E}{1 + \dfrac{H}{R_\oplus}}, \end{aligned} \tag{5}$$

where $R_\oplus$ is the Earth's radius.

We use Center for Orbit Determination in Europe (CODE) TEC time series (Schaer, 1999)[4] with a resolution of $5^\circ \times 2.5^\circ \times 2^h$. This resolution is relatively coarse and accounts only for a part of the signal. Therefore, our results of processing MOJAVE results are affected by systematic errors caused by the residual ionosphere.

In order to quantify the residual ionospheric signal, we process dual-band RDV&CN data set. For the purpose of this study, we consider that the ionospheric free linear combination of X and S band group delays has no ionospheric contribution. We can form the differences between the ionospheric contribution computed from TEC maps and from X and S band group delays and investigate the properties of this stochastic process.

Solving for zenith path delay in the neutral atmosphere will pick up a portion of the slowly varying bias, but the ionospheric fluctuations at scales less than several hours will propagate to residuals. We can try to characterize stochastic properties of the residual signal. The ionospheric path delay fluctuation is a non-stationary process. From the general results or turbulence theory, we can expect that fluctuations at scales x will be related to fluctuations at scales y via a power law. Therefore, we did the following:

First, we computed the mean differences $d_{gv} = \tau_{ig} - \tau_{iv}$ between the ionospheric path delay at X band computed from TEC maps (τ_{ig}) and from VLBI dual band observables (τ_{iv}) for every baseline and every experiment in RDV&CN dual-band dataset, and then we subtracted the mean value from d_{gv}. The mean value is the sum of the bias between TEC maps and VLBI ionospheric path delay and instrumental delay in VLBI hardware where the instrumental delay may be greater than the ionospheric signal. Since the instrumental delay is not calibrated, the mean value of d_{gv} is meaningless. Then we computed the rms over d_{gv}. We discarded the data with clock jumps that may happen at only one band. We got time series of rms(d_{gv}) and we examined empirical relationships of rms(d_{gv}) with other statistics. We found that rms^2(d_{gv}) has a linear dependence with rms(τ_{ig}). The power law dependence between d_{gv} and τ_{ig} was expected, but the power law coefficient, 2, is purely empirical. Fig. 5 demonstrates the time series of d_{gv} and their fit.

We can compute the rms of the ionospheric errors at a given baseline of a given experiment via

$$\mathrm{rms}(d_{gv}) = \sqrt{\rho\ \mathrm{rms}(\tau_{ig})}, \tag{6}$$

where ρ is the empirical coefficient determined from fitting (see Fig. 5) equal to 12.8 ps and the rms is ex-

[4] Available at ftp://ftp.aiub.unibe.ch/CODE

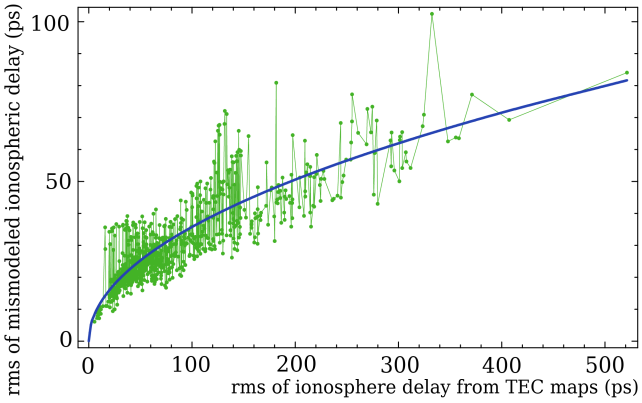

Fig. 5 The rms of the errors in ionospheric path delay as a function of rms of the variations of group delays derived from TEC maps (green dots). The solid blue line shows a regression in a form of the power law 1/2.

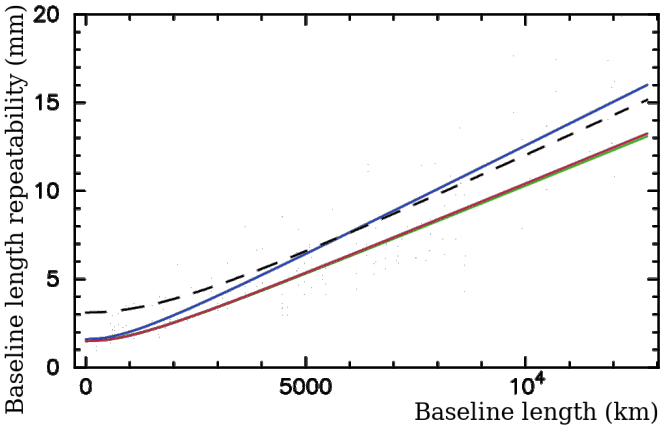

Fig. 6 The dependencies of baseline length repeatability fits on the baseline length. Upper blue curve shows the baseline repeatability for the X band only "bx" solution that uses GNSS TEC maps. Two lower very close curves, red and green, show the baseline length repeatability for the "bu" solution that shows the effect of mismodeled ionosphere on Ku band observable, and the reference dual band solution. The dashed black line shows the baseline length repeatability from the MOJAVE solution.

pressed in ps. This empirical relationship allows us to predict the second moment of the residual noise after we perform data reduction for the ionospheric contribution using the TEC maps. One can expect that if the TEC variance is greater, the residual errors are also greater. Expression (6) shows how much greater.

We have computed baseline-dependent additive noise due to mismodeled ionosphere for every baseline and every experiment of MOJAVE program using τ_{ig}. We added that noise to the a priori group delay errors in quadrature and computed new weights. We ran several baseline solutions, computed baseline repeatabilities, and compared them with the reference dual-band solution using RDV&CN data. In solution "bx" we used the ionosphere-free computations of group delays, added the contribution of the ionosphere τ_{iu} and processed this data the same way as MOJAVE data, i.e. performing data reduction for the ionosphere using CODE TEC maps and inflating a priori group delay uncertainties for the additional noise due to mismodeling the ionosphere. In the second solution "bu" we simulated how the deficiency of CODE TEC model would alter RDV&CN solution, as if these experiments ran at 15.3 GHz instead of 2.3/8.6 GHz. To achieve this, we re-scaled τ_{iu} by the square of the frequency ratio $(8.64/15.28)^2 \approx 0.32$. Fig. 6 shows fit in a form $\sqrt{a^2 + (b\,L)^2}$ for all these solutions. The baseline length repeatability from MOJAVE solution is shown by the dashed line.

We found that the impact of the mismodeling ionosphere on the baseline length repeatability of Ku band VLBA data collected in 2016–2020 during Solar minimum is negligible. Therefore, an increase in the baseline length repeatability from a geodetic solution using the MOJAVE dataset with respect to the reference dual-band RDV&CN solution cannot be explained by the unaccounted contribution of the ionosphere. We should also caution that this result should not be extrapolated to any other estimated parameter, such as source position, and should not be extrapolated to epochs of the Solar maximum.

4.3 Simulations

To touch the effect of source structure we run simulations of the observations. In the simulation tool of VieVS (Pany et al., 2011) we create the artificial group delay as:

$$\tau_{gr} = \tau_{mod} + \tau_{clk} + \tau_{zwd} + \tau_{wn}. \quad (7)$$

We add to the theoretically computed time delay (τ_{mod}) three stochastic error sources caused by the troposphere (τ_{zwd}), station clock (τ_{clk}) and measurement errors of the receiving system (τ_{wn}). For simulation of zenith wet delays VieVS using **the model of** Nilsson and Haas (2007). **In the framework of that approach we considered that the atmospheric turbulence for every station is described with a structure function** with $C_n = 1.8 \cdot 10^{-7}\mathrm{m}^{-1/3}$ for refractive index structure constant, $H = 2$ km for effective height, and constant wind velocity $v = 8$ m/s towards East. ~~which is based on the citetTreuhaft87 turbulence model~~. **Then we computed the covariance matrix between group delays each pair of observations of a given station and used them for computation of the full weight matrices under assumption that the atmospheric turbulence is a stationary process.**-

The simulation of station clocks was performed with

Corr 29
Corr 30
Corr 31

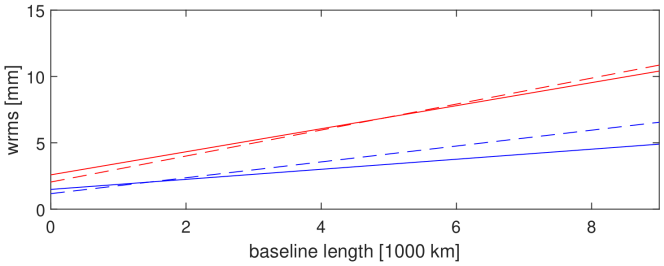

Fig. 7 Difference between the wrms of baseline length from simulated (dashed line) minus real observations (solid line). The upper red lines show the baseline lenght repeatability from analysis and simulation of MOJAVE-5 data. The low blue lines shows results of analysis and simulation of RV+CN data.

an Allan standard deviation of $1 \cdot 10^{-14}$ at 50 min, and we applied 20 ps for white noise. ~~This means that errors coming from the structure of radio sources are not included in the simulated delays.~~ **We did not include modeling source structure into simulation.-**

Corr 32

We have computed baseline length repeatabilities from simulated rv+cn and MOJAVE-5 datasets. The regression curves in a form $\sqrt{A^2 + (b\,L)^2}$ for simulated and real data are shown in Figure ??. We see from these plots that simulation results exhibit the same disparity in repeatabilities between MOJAVE-5 and rv+cn data as we saw in observations. Simulation results show even deeper disparity. Both datasets have different formal uncertainties that are computed using the law of error propagation based on the scan duration and a priori telescope sensitivities, but the same stochastic model. Since the the formal uncertainties for most of the observations are lower than the white noise and correlated atmospheric noise added during simulations, the stochastic observation model used in simulation is almost the same. This finding pinpoints the origin of discrepancies: differences in schedules. The main factor that affects baseline lengths is the spread of observation over low and high elevations over short periods of time. Since atmospheric path delay an clock function are modeled in a form of an expansion over the B-spline basis with a time span 20–60 minutes, in order for these two group of nuisance parameters be decorrelated, observation at significantly different elevations are required. Figure 7 shows that the spread of observations over elevations for geodetic experiment rv119 is noticeably wider, and observations at elevations below 30° **are much more often.**

Corr 33

4.4 Insight on the possible contribution of the source structure

Fig. 8 shows images of the three most observed sources in bl229aa (0636+680, 0210+515 and 0128+554) and in rv119 (2229+695, 0345+460, 0529+483) which are the first sessions of our datasets. We computed the so-called Structure Index (SI) introduced by Fey and Charlot (1997) for all sources observed in bl229aa. For that calculation we used maps provided by MOJAVE team[5] and split the sources in the four SI groups according to the median value of calculated structure delay corrections. ~~Out of the~~ **Among** 30 sources observed in bl229aa, 3 sources have SI 1, 14 sources SI 2, 8 sources SI 3, and 5 sources have the highest SI 4. Fig. 9 shows post fit residuals in session bl229aa for real observations v_{real} (lower plots) and for simulated observations v_{sim} (upper plots). As an example, we highlighted the most observed source 0636+680 in this session which has structure index 2 and 0128+554 with structure index 4. The comparison shows that the scatter of delay residuals for 0636+680 is similar to real and simulated observations and reaches in terms of rms 29.6 ps and 29.3 ps, respectively. The rms of delay residuals from source 0128+554 with extended structure is 2.5 times larger from real observations compared to the simulated ones, i.e., 72.3 ps and 27.4 ps, respectively. We computed the rms of delay residuals for every source in the bl229aa experiment and built the difference between the rms from real and simulated observations. The median value of the rms difference was built as

Corr 34

$$\Delta\mathrm{rms}_{\mathrm{med}} = \mathrm{median}(\mathrm{rms}(v_{real}) - \mathrm{rms}(v_{sim})) \qquad (8)$$

over each source group with respective structure index. The obtained median values are summarized in Table 8. It is obvious that with increasing source structure index the difference between simulated and real delay residuals is raising since the structure delay is not modeled in the simulated observations. With the SI 1 taken as a reference, the rms of the delay residuals increases by about 36 ps for sources with SI 4. ~~The better performance of real measurements~~ **The lower wrms of postfit residuals from processing real observations** for sources with low structure **indices** (SI 1 and SI 2) compared to the simulated observations as it is given by the negative $\Delta\mathrm{rms}_{\mathrm{med}}$ ~~is caused probably by the fact that we applied identical turbulence parameters to all stations in the network instead of using a site-dependent setup what creates slightly unrealistic environment where e.g. the wind is blowing towards the same direction at all telescopes in the network.~~ **is due to the fact the excessive noise due to source structure is less than**

Corr 35
Corr 36

[5] Available at https://www.physics.purdue.edu/MOJAVE

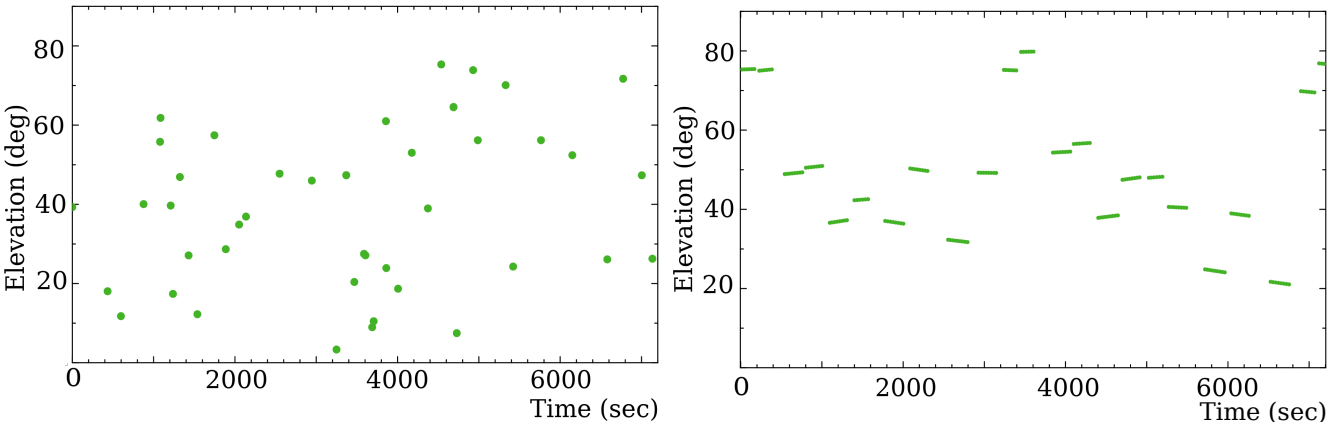

Fig. 8 Distribution of observations over elevations for station NL-VLBA within first two hours of an experiment. *Left:* Geodetic experiment rv119. *Right:* Astronomical experiment bl229bf.

Table 8 Median of rms differences between delay residuals from real and simulated observations in bl229aa. Sources are divided in four groups according to their structure index.

SI	N_{sou}	Δrms$_{\rm med}$ [ps]
1	3	-11.3
2	14	-6.6
3	8	9.0
4	5	25.0

random Gaussian noise with the rms of 20 ps that had been added to simulated path delay in our simulation.

Corr 37

We see that the source structure contribution increases the rms of the postfit residuals but such an increase even for a subset of sources with strong radio jets picked up for an astronomical program does not have a noticeable impact on baseline length repeatability. Source structure causes not only random by also systematic errors that in a case of baseline length repeatability are insignificant. We exercise a caution to extrapolate these result to another metrics such the EOP and source position estimates. This requires a further investigation that is beyond the scope of present work.

Corr 38

~~In order to examine the source structure contribution to the baseline length repeatability we simulated all sessions from our two datasets and analyzed them in the same manner as the real measurements. Fig. 10 shows the differences between the baseline length scatter from the simulated w.r.t. real observations in the MOJAVE data set (red crosses) and RDV&CN sessions (blue x-signs) where the negative values mean better baseline length repeatability for simulated observations. It is rather surprising that the difference between the simulated and real baseline length scatter is similar for MOJAVE and RDV&CN dataset and the neglecting of source structure in the simulated observations does not have a more prominent effect on the baseline scatter in the MOJAVE dataset. On the other hand, since our network consist from VLBA telescopes only, the shorter baselines do not observe much of the radio source structure.~~

5 Conclusions

The most limiting factor for the usage of bl229aa MOJAVE-5 sessions for geodetic VLBI is the schedule of the sessions which determines the sky coverage over the stations.

We have processed 33 diurnal astronomical observing VLBI sessions at 15 GHz under program MOJAVE-5 and 28 diurnal VLBI geodetic dual-band observing sessions at 2 and 8 GHz under programs RV and CN. Both observing sessions ran the same ten station VLBA network with baseline lengths in a range from 237 to 8612 km at approximately the same time interval 2016–2020.

Corr 39

We found that while the wrms of post-fit residuals from MOJAVE-5 program was lower than from RV+CN, 16.37 ps versus 26.13 ps, important metrics of the geodetic quality of solutions, such as baseline length repeatability and wrms of the differences of the EOP with respect to the reference IERS C04 times series were a factor 1.3 to 1.8 worse. We have investigated the origin of these discrepancies. We found that modeling the ionospheric path delay using the GNSS TEC maps was adequate for processing 15 GHz data during the solar minimum, and the errors of these map did not affect baseline length repeatability at a noticeable level. We have in-

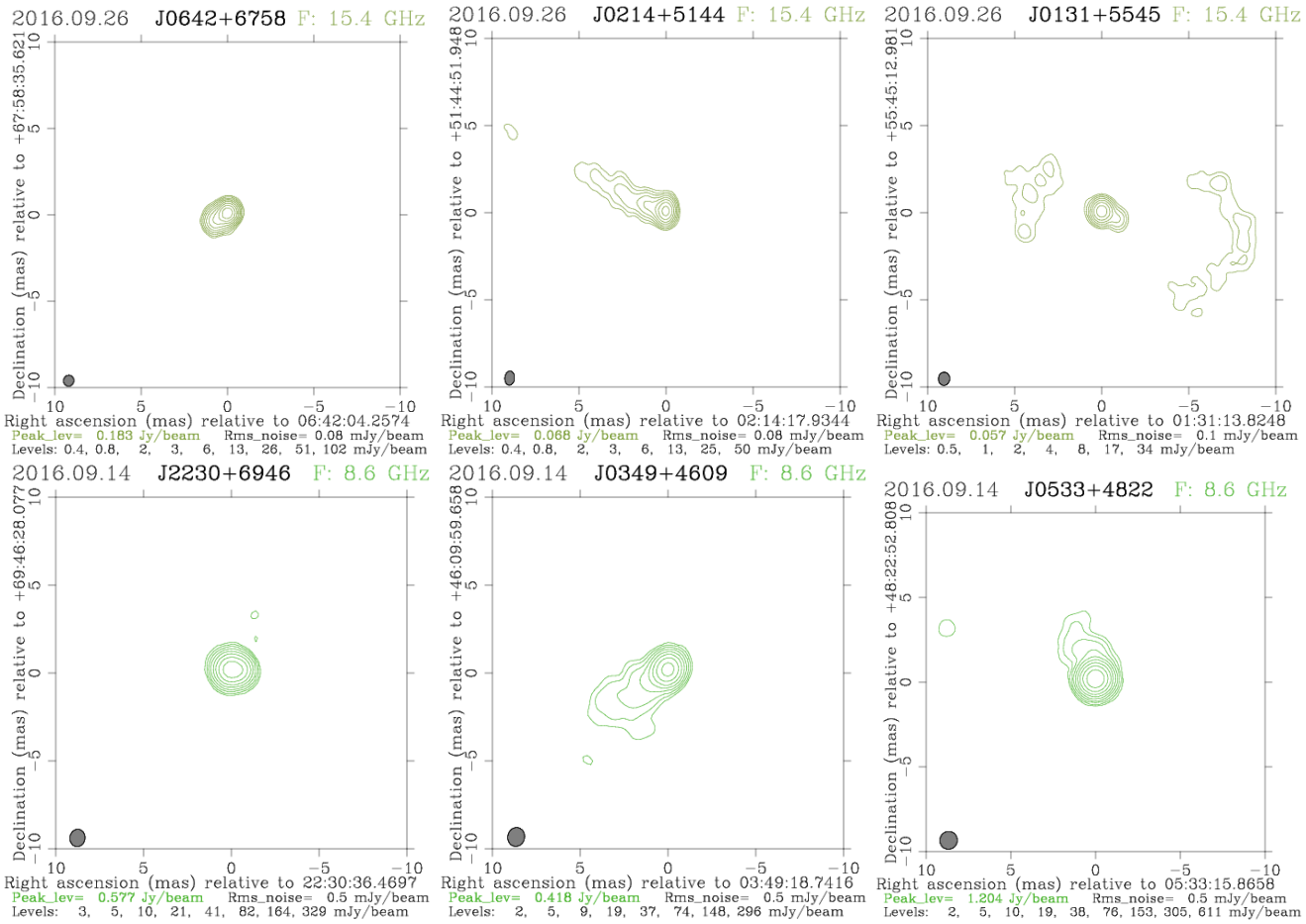

Fig. 9 Images of three most observed sources (0636+680 with SI 2, 0210+515 with SI 3 and 0128+554 with SI 4) in the bl229aa MOJAVE experiment (upper plots) and in the rv119 experiment at X band (lower plots: 2229+695 with SI 2, 0345+460 with SI 2, 0529+483 with SI 2). **We have produced images from rv119 ourselves. The images in FITS format are available in the Astrogeo VLBI FITS image database** http://asteogeo.org/vlbi_images. Information about the structure index for the X band sources was taken from the Bordeaux VLBI Image Database available at http://bvid.astrophy.u-bordeaux.fr.

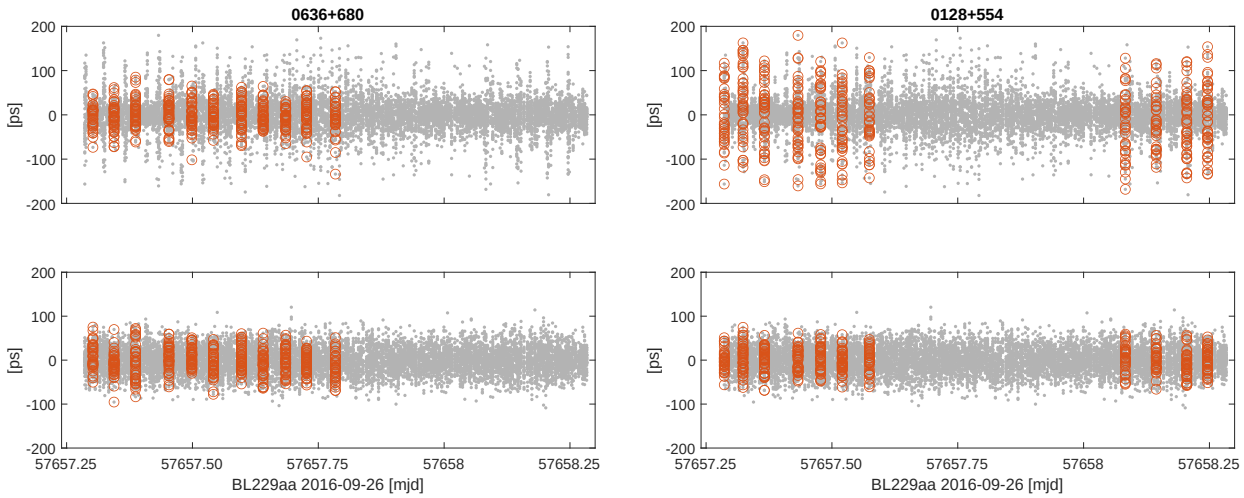

Fig. 10 Post fit residuals in session bl229aa for real (upper plots) and simulated (lower plots) observations. Highlighted are sources 0636+680 with SI 2 and 0128+554 with SI 4.

vestigated whether the source structure can be a factor, since MOJAVE-5 targeted objects with strong radio jets and we did not find evidence it affected baseline length repeatability. Finally, we ran solutions with simulated right hand sides for both MOJAVE-5 and RV+CN programs. The stochastic model used for these simulations was almost the same. And we able to reproduce discrepancies in baseline lengths.

Corr 40

The major factor that caused discrepancies in baseline length repeatability was more agile schedule of rv+cn experiments that included more scans at low and high elevations at short intervals 0.5–2 hours than the astronomical experiment.

Corr 41

Although the use of single-band astronomical VLBI data from MOJAVE-5 program for geodesy provided less accurate results than the use of VLBI data from a the dedicated geodesy RV+CN campaign, the baseline length repeatability is still below 1 ppb. This gives us a rough estimate of the impact of remaining systematic errors that are specific for MOJAVE-5. This very low level of systematic errors confirms that MOJAVE-5 dataset is an excellent testbed for investigation of the effect of source structure on astrometry and geodesy in full detail.

Corr 42

Acknowledgements HK works within the Hertha Firnberg position T697-N29, funded by the Austrian Science Fund (FWF). This research has made use of data from the MOJAVE database that is maintained by the MOJAVE team (Lister et al., 2018). The VLBA is operated by the National Radio Astronomy Observatory, which is a facility of the National Science Foundation, and operated under cooperative agreement by Associated Universities, Inc. **The authors acknowledge use of the Very Long Baseline Array under the US Naval Observatory's time allocation. This work supports USNO's ongoing research into the celestial reference frame and geodesy. This research has made use of data from the MOJAVE database that is maintained by the MOJAVE team.**

Corr 43

References

Anderson JM, Xu MH (2018) Source structure and measurement noise are as important as all other residual sources in geodetic vlbi combined. Journal of Geophysical Research: Solid Earth 123(11):10,162–10,190, DOI https://doi.org/10.1029/2018JB015550

Böhm J, Böhm S, Boisits J, Girdiuk A, Gruber J, Hellerschmied A, Krásná H, Landskron D, Madzak M, Mayer D, McCallum J, McCallum L, Schartner M, Teke K (2018) Vienna VLBI and Satellite Software (VieVS) for Geodesy and Astrometry. Publications of the Astronomical Society of the Pacific 130(986):044503, DOI 10.1088/1538-3873/aaa22b

Fey AL, Charlot P (1997) Vlba observations of radio reference frame sources. ii. astrometric suitability based on observed structure. ApJS 111:95–142, DOI 10.1086/313017

Greisen EW (2003) AIPS, the VLA, and the VLBA. In: Heck A (ed) Information Handling in Astronomy - Historical Vistas, Astrophysics and Space Science Library, vol 285, p 109, DOI 10.1007/0-306-48080-8_7

Hawarey M, Hobiger T, Schuh H (2005) Effects of the 2nd order ionospheric terms on VLBI measurements. Geophys Res Lett 32:L11304, DOI 10.1029/2005GL022729

Helmboldt JF, Taylor GB, Tremblay S, Fassnacht CD, Walker RC, Myers ST, Sjouwerman LO, Pearson TJ, Readhead ACS, Weintraub L, Gehrels N, Romani RW, Healey S, Michelson PF, Blandford RD, Cotter G (2007) The VLBA imaging and polarimetry survey at 5 GHz. Astrophys. J.658(1):203–216, DOI 10.1086/511005, URL https://doi.org/10.1086%2F511005

Krásná H, Gordon D, de Witt A, Jacobs CS, Soja B (2019) Earth Orientation Parameters Estimated From K-band VLBA Measurements. In: Haas R, Garcia-Espada S, Lopez Fernandez J (eds) Proceedings of the 24th European VLBI Group for Geodesy and Astrometry Working Meeting, Chalmers University of Technology, vol 24, pp 238–242, DOI 10.7419/162.08.2019, iSBN:978-84-416-5634-5

Lister ML, Aller MF, Aller HD, Hodge MA, Homan DC, Kovalev YY, Pushkarev AB, Savolainen T (2018) MOJAVE. XV. VLBA 15 GHz Total Intensity and Polarization Maps of 437 Parsec-scale AGN Jets from 1996 to 2017. ApJS 234(1):12, DOI 10.3847/1538-4365/aa9c44

Nilsson T, Haas R (2007) Simulations of atmospheric path delays using turbulence models. In: Böhm J, Pany A, Schuh H (eds) Proceedings of the 18th European VLBI Group for Geodesy and Astrometry Working Meeting, Technische Universität Wien, pp 175–180, iSSN: 1811–8380

Pany A, Böhm J, MacMillan D, Schuh H, Nilsson T, Wresnik J (2011) Monte carlo simulations of the impact of troposphere, clock and measurement errors on the repeatability of vlbi positions. Journal of Geodesy 85:39–50, DOI 10.1007/s00190-010-0415-1

Petrov L (2007) The empirical Earth rotation model from VLBI observations. Astron. & Astrophys.467(1):359–369, DOI 10.1051/0004-6361:20065091, astro-ph/0611781

Petrov L (2011) The Catalog of Positions of Optically Bright Extragalactic Radio Sources OBRS-1.

Astronom. J.142:105, DOI 10.1088/0004-6256/142/4/105, 1103.2840

Petrov L (2013) The Catalog of Positions of Optically Bright Extragalactic Radio Sources OBRS-2. Astronom. J.146:5, DOI 10.1088/0004-6256/146/1/5, 1301.5407

Petrov L, Kovalev YY (2017) Observational consequences of optical band milliarcsec-scale structure in active galactic nuclei discovered by Gaia. Mon. Not. Roy. Astron. Soc.471:3775–3787, DOI 10.1093/mnras/stx1747, 1704.07365

Petrov L, Taylor GB (2011) Precise Absolute Astrometry from the VLBA Imaging and Polarimetry Survey at 5 GHz. Astronom. J.142:89, DOI 10.1088/0004-6256/142/3/89, 1106.2382

Petrov L, Gordon D, Gipson J, MacMillan D, Ma C, Fomalont E, Walker RC, Carabajal C (2009) Precise geodesy with the Very Long Baseline Array. Journal of Geodesy 83:859–876, DOI 10.1007/s00190-009-0304-7, 0806.0167

Petrov L, Kovalev YY, Fomalont EB, Gordon D (2011) The Very Long Baseline Array Galactic Plane Survey—VGaPS. Astronom. J.142:35, DOI 10.1088/0004-6256/142/2/35, 1101.1460

Petrov L, Kovalev YY, Fomalont EB, Gordon D (2011) The Very Long Baseline Array Galactic Plane Survey–VGaPS. The Astronomical Journal 142(2):35, DOI 10.1088/0004-6256/142/2/35

Schaer S (1999) Mapping and predicting the Earth's ionosphere using the Global Positioning System. Geod-Geophys Arb Schweiz, Vol 59, 59, http://ftp.aiub.unibe.ch/papers/ionodiss.ps

Shabala S, McCallum JN, Plank L, Böhm J (2015) Simulating the effects of quasar structure on parameters from geodetic vlbi. J Geod 89:873—-886, DOI 10.1007/s00190-015-0820-6

Sovers OJ, Charlot P, Fey AL, Gordon D (2002) Structure Corrections in Modelling VLBI Delays for RDV Data. In: Vandenberg NR, Baver KD (eds) IVS GM Proceedings, NASA, pp 243–247, nASA/CP-2002-210002

Tornatore V, Charlot P (2007) The impact of radio source structure on european geodetic vlbi measurements. J Geod 81:469—-478, DOI 10.1007/s00190-007-0146-0

Zeppenfeld G (1993) Einflüsse der Quellenstruktur in der Praxis der geodätischen VLBI. Mitteilungen Geod Institut Rheinischen Friedrich-Wilhelms-Universitaets Bonn 80